Effect of the nonlinear displacement-dependent characteristics of a hydraulic damper on high-speed rail pantograph dynamics

Wenlin Wang[a, b, c*], Yuwen Liang[b], Weihua Zhang[c], Simon Iwnicki[d]

[a] School of Mechanical Engineering, Dongguan University of Technology, Dongguan 523808, P. R. of China

[b] College of Mechanical and Vehicle Engineering, Hunan University, Changsha 410082, P. R. of China

[c] State Key Laboratory of Traction Power, Southwest Jiaotong University, Chengdu 610031, China

[d] Institute of Railway Research, University of Huddersfield, Huddersfield HD1 3DH, UK

Abstract: A new simplified-parametric model is proposed to describe the nonlinear displacement-dependent damping characteristics of a railway pantograph hydraulic damper and validated by the experimental results in this study. Then, a full mathematical model of the pantograph-catenary system, which incorporates the new pantograph damper model, is established to simulate the effect of the damping characteristics on the pantograph dynamics. The simulation results show that large F_{const} and C_0 in the pantograph damper model can improve both the raising performance and contact quality of the pantograph, whereas a large C_0 has no obvious effect on the lowering time of the pantograph; the nonlinear damping characteristics described by the second item in the new damper model have dominating effects on the total lowering time, maximum acceleration and maximum impact acceleration of the pantograph. Thus, within the constraint of total lowering time, increasing the second item damping characteristics of the damper will obviously improve the lowering performance of the pantograph and reduce excessive impact between the pantograph and its base frame. The proposed concise pantograph hydraulic damper model appears to be more complete and accurate than the previous single-parameter model, so it is more useful in the context of pantograph-catenary dynamics simulation and further parameter optimizations. The obtained simulation results are also valuable and instructive for further optimal specification of railway pantograph hydraulic dampers.

Keywords: Pantograph hydraulic damper; displacement-dependent; nonlinear damping characteristics; pantograph-catenary dynamics; contact quality; raising and lowering performance

1. Introduction

The pantograph is a key device in the current collection by modern high-speed rail vehicles [1]; an optimal design of the structural and component parameters of the pantograph will improve the pantograph-

---

* Corresponding author at: School of Mechanical Engineering, Dongguan University of Technology, Dongguan 523808, Guangdong Province, PR China. Tel.: +86 769 22861122.

E-mail address: pianowwl@163.com (Wenlin Wang).

catenary interaction and enable more stable current collection. A hydraulic damper is often installed between the base frame and the lower arm mechanism of a pantograph, as illustrated in Fig. 1. When the pantograph is lowered, the damper is extended; when the pantograph is raised, the damper is compressed. The hydraulic damper is a crucial component in improving the pantograph-catenary interaction quality and obtaining the ideal raising and lowering performance of the pantograph.
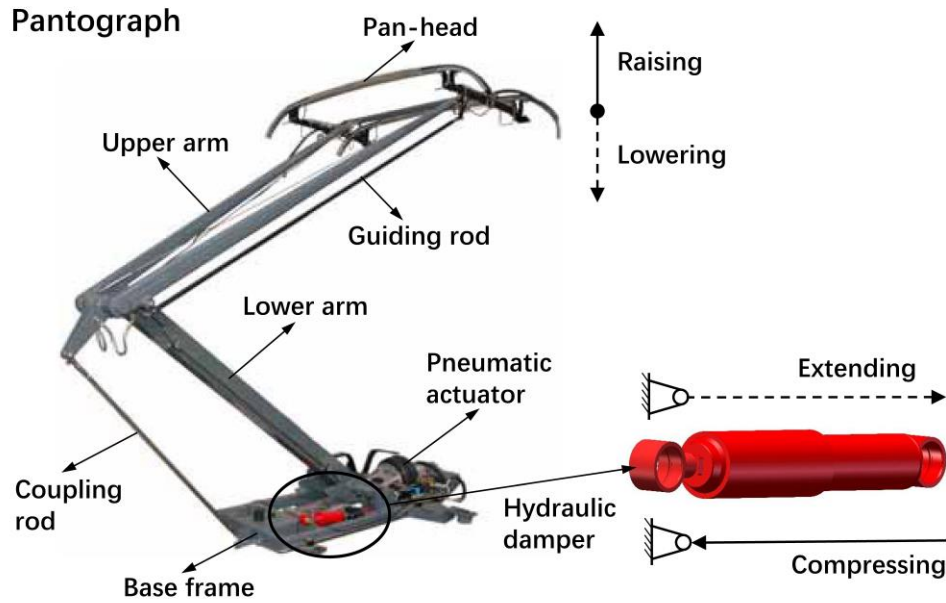

Fig. 1 A simple illustration of the motions of a high-speed rail pantograph and its hydraulic damper

Previous studies have been performed to model the nonlinear characteristics of railway hydraulic dampers and analyse their effects on the yaw motion, stability [2–4] and riding comfort [5] of rail vehicle systems. Oh, et al. [6] introduced magneto-rheological dampers in the semi-active control of the rail vehicle secondary suspension. Stein, et al. [7] used an adjustable damper in the seat suspension of a locomotive driver to reduce fatigue and pursue better comfort of the locomotive driver. Croft, et al. [8] modelled and predicted the effect of rail dampers on the wheel-rail interaction and rail roughness growth.

Pombo and Ambrósio [9] studied the effects of the pan-head mass, pan-head suspension stiffness and base frame damping on the pantograph-catenary interaction quality by establishing a lumped-mass linear dynamic model of the pantograph. In the pantograph model, the hydraulic damper was considered a single-parameter linear model with the damping coefficient as the only parameter. In many similar studies, in both lumped-mass [10–15] and multibody [16–18] pantograph models, the hydraulic damper was treated as a single-parameter model.

Zhou and Zhang [19] optimized the pantograph parameters using the sensitivity analysis and experience, and the optimal results were experimentally validated. Similar design optimizations [20–23] of the

2

pantograph parameters were performed using automatic algorithms or robust design techniques. However, in these works, the pantograph models are almost lumped-mass linear ones, where the hydraulic damper is also considered a single-parameter model.

Thus:

(1) Research on modelling the nonlinear displacement-dependent characteristics of the pantograph hydraulic damper is notably limited.

(2) In current studies on the pantograph-catenary interaction and parameter design optimization of the pantograph and catenary system, the hydraulic damper was considered a single-parameter linear model. The single-parameter linear model is notably different from the actual nonlinear displacement-dependent characteristics. In addition, during the raising or lowering process of the pantograph, the damper angle changes with the motion of the framework, so there is the problem of effective damping. Thus, the current damper model appears incomplete, and the accuracy must be improved.

(3) Most existing works concern the problems of the pantograph-catenary interaction, but the effect of component characteristics, e.g., the hydraulic damper characteristics, on the raising and lowering performance of the pantograph is hardly addressed.

In this work, a new simplified-parametric model is proposed to describe the nonlinear displacement-dependent damping characteristics of the pantograph hydraulic damper and validated by experimental results. Then, a full mathematical model of the pantograph-catenary system, which incorporates the new pantograph damper model, is established to simulate the effect of the damping characteristics on the pantograph dynamics, and valuable results are obtained. The concise pantograph hydraulic damper model appears to be more complete and accurate than previous single-parameter model, so it is more useful in the context of pantograph-catenary dynamics simulation and parameter optimization. The obtained simulation results are also valuable and instructive for further optimal specification of pantograph hydraulic dampers.

The paper is structured as follows: a full mathematical modelling of the pantograph-catenary system with a new damper model is performed in Section 2, the effect of the damper characteristics on the pantograph dynamics is simulated in Section 3, and conclusions are drawn in the final section.

2. Mathematical modeling of the pantograph-catenary system with a new damper model

Figure 2 schematically illustrates the configuration, geometry and parameters of the pantograph-catenary system. The structures of the upper arm, lower arm, guiding rod, coupling rod and hydraulic damper are considered a united multibody mechanism, i.e., the framework; the pantograph head includes mass m_h and a suspension with stiffness k_h and damping c_h; the pantograph head is connected with the framework by joint E. The moving pantograph-catenary interaction is simplified as a variable stiffness k_c,
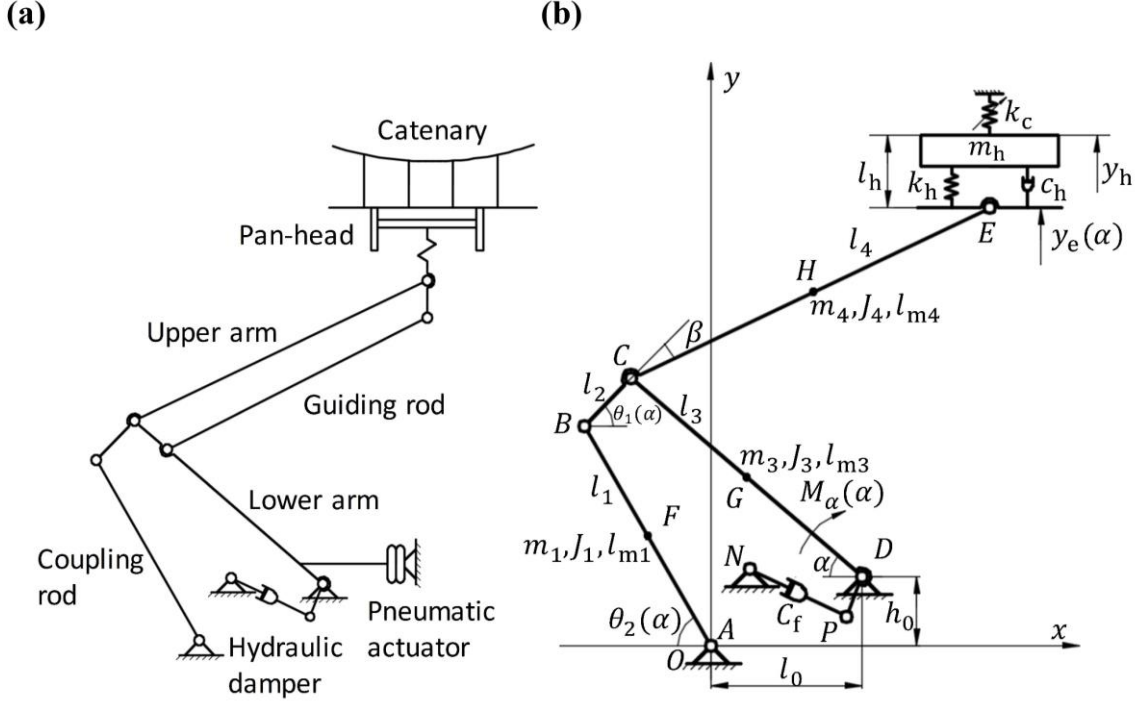
Fig. 2 Schematic illustrations of the configuration (a), geometry and parameters (b) of the pantograph-catenary system

so the dynamic interaction force between the pan-head and the catenary can be readily obtained.

2.1. Multibody dynamic model of the pantograph framework

2.1.1 Relations among key kinematic parameters

To model the multibody dynamics of the pantograph framework, it is necessary to first deduce the kinematic relations among the components of the framework. Using the parameters and coordinates in Fig. 2(b) and only considering the vertical motion of the pantograph, it is easy to deduce the positions and angles of all nodes in the framework in terms of raising angle α of the lower arm.

For example, the raising angle of the coupling rod in terms of α can be formulated by

$$\theta_2(\alpha) = 2\arctan\frac{k_2 + \sqrt{-k_1^2 + k_2^2 + k_3^2}}{k_1 + k_3} \tag{1}$$

where

$$\begin{cases} k_1 = l_2^2 - l_1^2 - l_3^2 - h_0^2 - l_0^2 + 2l_0l_3\cos\alpha - 2h_0l_3\sin\alpha \\ k_2 = -2l_1l_3\sin\alpha - 2h_0l_1 \\ k_3 = -2l_1l_3\cos\alpha + 2l_0l_1 \end{cases} \tag{2}$$

and the raising angle of the connection rod BC in terms of α can also be written as

$$\theta_1(\alpha) = \arctan \frac{-l_1 \sin \theta_2 + h_0 + l_3 \sin \alpha}{l_1 \cos \theta_2 + l_0 - l_3 \cos \alpha} \tag{3}$$

The displacement of joint E, which is also a crucial parameter, can be deduced as follows

$$y_e(\alpha) = h_0 + l_3 \sin \alpha + l_4 \sin(\theta_1 - \beta) \tag{4}$$

2.1.2 Multibody dynamic model of the pantograph framework

In Fig. 2(b), all rods are considered rigid bodies; because the masses of the guiding rod and connection rod BC are small, the guiding rod is negligible, and the connection rod BC can be considered a rod with no mass and no moment of inertia. Thus, the multibody dynamics of the pantograph framework can be described by the following Lagrange differential equation

$$\frac{d}{dt}\left(\frac{\partial L}{\partial \dot{\alpha}}\right) - \frac{\partial L}{\partial \alpha} = G_F \tag{5}$$

where L is the Lagrangian function and $L=T-U$; T is the kinetic energy of the framework; U is the potential energy of the framework when the potential energy in the plane across point A is considered to be zero. Thus, according to Fig. 2(b), we obtain

$$T = \frac{1}{2}J_1\dot{\theta}_2^2 + \frac{1}{2}J_3\dot{\alpha}^2 + \frac{1}{2}J_4\dot{\theta}_1^2 + \frac{1}{2}m_4[l_3^2\dot{\alpha}^2 + 2l_3 l_{m4}\dot{\alpha}\dot{\theta}_1\cos(\alpha + \theta_1 - \beta)] \tag{6}$$

and

$$U = m_1 g l_{m1} \sin \theta_2 + m_3 g(l_{m3} \sin \alpha + h_0) + m_4 g[h_0 + l_3 \sin \alpha + l_{m4} \sin(\theta_1 - \beta)] \tag{7}$$

In Eq. (5), G_F is the generalized force, which includes interaction forces from the pantograph head and hydraulic damper and the uplift moment from the pneumatic actuator. According to the principle of virtual work, G_F can be formulated [24] by

$$G_F = M_\alpha + k_4[k_h(y_h - y_e - l_h) + c_h(\dot{y}_h - \dot{y}_e) + m_h g] - F_d k_5 \tag{8}$$

where coefficients k_4 and k_5 are defined as variations of the displacement of joint E y_e to α and hydraulic damper length s to α, respectively; k_4 and k_5 are written as

$$k_4 = \frac{\delta y_e}{\delta \alpha}, \ k_5 = \frac{\delta s}{\delta \alpha} \tag{9}$$

Referring to Fig. (3), we can calculate the dynamic damper length s in terms of α in Eq. (9) as follows

$$s(\alpha) = \sqrt{[x_d + l\cos(\alpha + \gamma)]^2 + [y_d + l\sin(\alpha + \gamma)]^2} \tag{10}$$

Thus, we substitute Eqs. (6)-(10) into Eq. (5) to obtain a dynamic model of the framework in terms of α

$$J_f(\alpha)\ddot{\alpha} + U_f(\alpha)\dot{\alpha}^2 + C_f(\alpha)\dot{\alpha} + F_f(\alpha) = M_\alpha(\alpha) \tag{11}$$

where the effective moment of inertia J_f of the framework, coefficient U_f, effective damping coefficient C_f of the framework, generalized force F_f of the framework and uplift moment M_α from the pneumatic actuator

5

can be described as follows

$$J_f(\alpha) = J_1 k_6{}^2 + J_3 + J_4 k_7^2 + m_4[l_3^2 + 2k_7 l_3 l_{m4} \cos(\alpha + \theta_1 - \beta)] \tag{12}$$
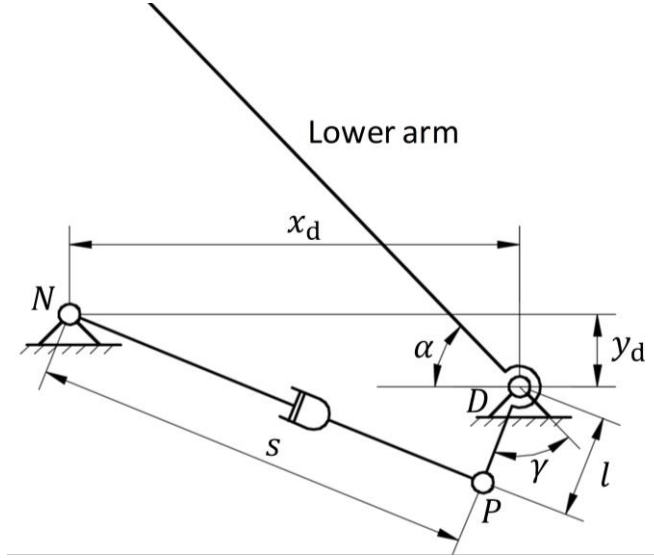

Fig. 3 Geometric parameters to calculate the motion of the hydraulic damper

$$U_f(\alpha) = J_1 k_6 k_8 + J_4 k_7 k_9 + m_4[k_9 l_3 l_{m4} \cos(\alpha + \theta_1 - \beta) - k_7(1 + k_7)l_3 l_{m4} \sin(\alpha + \theta_1 - \beta)] \tag{13}$$

$$C_f(\alpha) = \frac{d(F_d k_5)}{d\dot{\alpha}} \tag{14}$$

$$F_f(\alpha) = m_1 g l_{m1} k_6 \cos\theta_2 + m_3 g l_{m3} \cos\alpha + m_4 g[l_3 \cos\alpha + l_{m4} k_7 \cos(\theta_1 - \beta)] \\ + k_4[k_h(y_h - y_e - l_h) + c_h(\dot{y}_h - \dot{y}_e) + m_h g] \tag{15}$$

$$M_\alpha(\alpha) = m_1 g l_{m1} k_6 \cos\theta_2 + m_3 g l_{m3} \cos\alpha + m_4 g[l_3 \cos\alpha + l_{m4} k_7 \cos(\theta_1 - \beta)] + k_4(F_u + m_h g) \tag{16}$$

where coefficients k_6 and k_7 are defined as the variations of the coupling rod raising angle θ_2 to α and the angle of the connecting rod BC to horizontal line θ_1 to α, respectively; k_6 and k_7 are written as

$$k_6 = \frac{\delta\theta_2}{\delta\alpha}, \ k_7 = \frac{\delta\theta_1}{\delta\alpha} \tag{17}$$

Coefficients k_8 and k_9 are defined as

$$k_8 = \frac{dk_6}{d\alpha}, \ k_9 = \frac{dk_7}{d\alpha} \tag{18}$$

In the pantograph dynamics research, sometimes it is more interesting to study the dynamic model in terms of the displacement of joint E, i.e., y_e; hence, except for using Eq. (4), it is easy to deduce and use the following relations to transform α to y_e

$$\dot{\alpha} = \frac{1}{k_4}\dot{y}_e, \ \ddot{\alpha} = \frac{1}{k_4}\ddot{y}_e + \frac{k_{10}}{k_4^2}\dot{y}_e{}^2 \tag{19}$$

where coefficient k_{10} is defined as

$$k_{10} = -\frac{dk_4}{d\alpha} \tag{20}$$

2.2. Dynamic model of the pantograph head with catenary interaction

Referring to Fig. 2(b) and according to Newton's second law, the dynamic model of the pantograph head is written as

$$m_h \ddot{y}_h = -k_h(y_h - y_e - l_h) - c_h(\dot{y}_h - \dot{y}_e) - F_c \tag{21}$$

where the pantograph-catenary interaction force F_c can be further written as

$$F_c = \begin{cases} k_c(y_h - y_c), & y_h \geq y_c \\ 0, & y_h < y_c \end{cases} \tag{22}$$

where k_c is the changeable catenary stiffness and given by the following model [25]

$$k_c(v, t) = k_0[1 + a_1 \cos(\frac{2\pi v}{L_c}t) + a_2 \cos(\frac{2\pi v}{L_d}t) + a_3 \cos^2(\frac{2\pi v}{L_c}t) + a_4 \cos^2(\frac{\pi v}{L_c}t) + a_5 \cos^2(\frac{\pi v}{L_d}t)] \tag{23}$$

Eq. (23) describes the fluctuating stiffness of the catenary in terms of the pantograph moving speed and time; it is a law fitted from the finite element model [25] of the common Chinese catenary.

Thus, as shown in Fig. 2(b), the dynamics of the pantograph head and catenary are coupled by k_c; the dynamics of the pantograph head and framework are coupled by joint E, i.e., the dynamic forces from the pantograph head act on the framework through joint E, and in return the framework motions affect the pantograph head also through joint E.

2.3. Nonlinear displacement-dependent characteristics of the hydraulic damper

The pantograph damper has nonlinear displacement-dependent damping characteristics. Figs. 1 and 4(a) show that when the pantograph is in the normal working position, the damper has the shortest length, vibrates with very small amplitudes, and provides the pantograph with a small damping.

When the pantograph is lowered, the damper is extended and the fluids in the damper are displaced from the left chamber of the piston to the right chamber of the piston through the orifices in the rod. At the beginning of the extension, the damper produces small damping forces. However, with continuing extension of the damper, the orifices in the rod are sequentially obstructed by the guide seat, and the pressure in the left chamber of the piston increases, so the damper produces notably high damping forces to stop the pantograph to the vehicle roof.

When the pantograph is raised, the damper is compressed and the fluids in the damper are displaced from the inner tube to the reservoir through the foot valve with small resistances. In this process, the damper also provides the pantograph with a small damping.
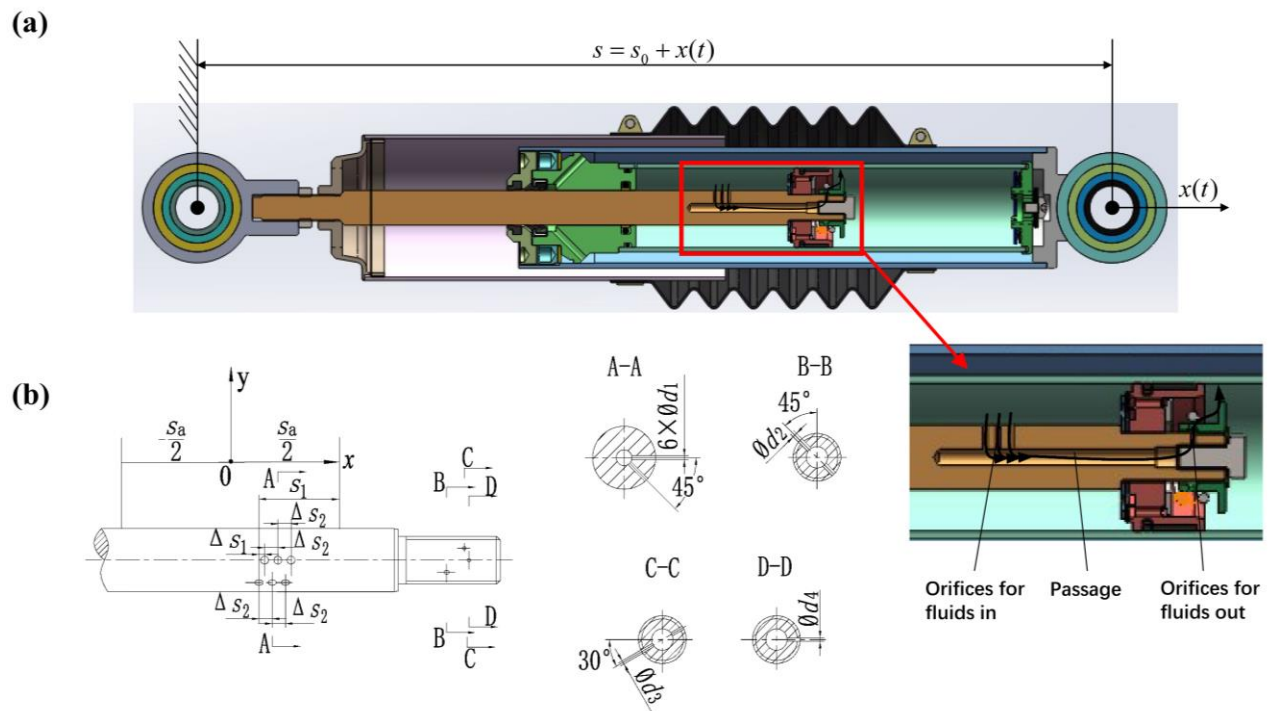

Fig. 4 (a) Cross-section of the pantograph damper; (b) engineering drawing of the cross-sections and dimensions of the orifices in the rod

A full parametric model of the pantograph damper has been built in the literature [26]; however, in the pantograph dynamics simulation, a simplified parametric model is wieldier and more efficient.

2.3.1 Damping performance in the extension stroke

During the extension stroke of the damper, referring to Fig. 4, it is easy to write the following fluid continuity equations

$$Q_{\text{work}} = A_{\text{x}} \dot{x}(t) = C_{\text{d1}} A_n \left[\frac{2}{\rho} (P - P_{\text{i}}) \right]^{1/2} \tag{24}$$

$$Q_{\text{work}} = C_{\text{d1}} A_{\text{f}} \left(\frac{2}{\rho} P_{\text{i}} \right)^{1/2} \tag{25}$$

where the pressure action area A_{x} of the piston during the extension stroke of the damper and the constant cross-section area A_{f} of the orifices in the rod for fluids outflow are written as

$$A_{\text{x}} = \frac{\pi}{4} (D^2 - d^2), \ A_{\text{f}} = \frac{\pi}{4} (2d_2^2 + 2d_3^2 + d_4^2) \tag{26}$$

The changeable cross-section area A_n of the orifices in the rod for fluids inflow is described by

$$A_n = \frac{\pi}{4} (d_0^2 + nd_1^2), \ n = 0,1,\cdots 6 \tag{27}$$

We combine Eqs. (24) and (25) to obtain

$$P = \frac{\rho A_{\text{x}}^2 (A_{\text{f}}^2 + A_n^2)}{2C_{\text{d1}}^2 A_{\text{f}}^2 A_n^2} \dot{x}^2(t) \tag{28}$$

Thus, the damping force during the extension stroke of the damper is

$$F_{\text{d}} = PA_{\text{x}} = \frac{\rho A_{\text{x}}^3 (A_{\text{f}}^2 + A_n^2)}{2C_{\text{d1}}^2 A_{\text{f}}^2 A_n^2} \dot{x}^2(t) \tag{29}$$

if defining a constant

$$k_{11} = \frac{\rho A_{\text{x}}^3}{2C_{\text{d1}}^2 A_{\text{f}}^2} \tag{30}$$

it is easy to obtain

$$F_{\text{d}} = k_{11} \left(1 + \frac{A_{\text{f}}^2}{A_n^2} \right) \dot{x}^2(t) \tag{31}$$

Therefore, the damping coefficient of the pantograph damper during extension can be written as

$$C_{\text{ext}} = k_{11} \left(1 + \frac{A_{\text{f}}^2}{A_n^2} \right) \dot{x}(t) \tag{32}$$

Eq. (32) indicates that the damping coefficient of the damper during extension is governed by its displacement in relation to parameter A_n, and its speed $\dot{x}(t)$.

2.3.2 Damping performance in the compression stroke

During the compression stroke of the damper, referring to Fig. 4, it is also easy to write the following

fluid continuity equation

$$Q_{\text{work}} = A_{\text{c}}\dot{x}(t) = C_{\text{d1}}\left(\frac{\pi}{4}d_0^{\,2}\right)\left(\frac{2}{\rho}P\right)^{1/2} + C_{\text{d2}}\left[2\pi r_{\text{s}}C_{\text{e}}C_{\text{w}}\big|_{r=r_s}\frac{P}{E(h_1^{\,3} + h_2^{\,3} + \cdots + h_n^{\,3})}\right]\left(\frac{2}{\rho}P\right)^{1/2} \tag{33}$$

where the pressure action area A_{c} of the piston during the compression stroke of the damper is written as

$$A_{\text{c}} = \frac{\pi}{4}d^2 \tag{34}$$

the amount of fluid that passes through the small constant orifice d_0 in the inner tube is very small and on a different scale, when compared with the amount of fluid that passes through the compression shim-stack valve in the foot valve assembly. Thus, if we neglect the flow relating to constant orifice d_0 in Eq. (33) and define a constant for the shim-stack valve

$$k_{12} = \frac{2\pi C_{\text{d2}}r_{\text{s}}C_{\text{e}}C_{\text{w}}\big|_{r=r_s}}{E(h_1^{\,3} + h_2^{\,3} + \cdots + h_n^{\,3})}\sqrt{\frac{2}{\rho}} \tag{35}$$

it is easy to solve Eq. (33) and obtain

$$P = \left(\frac{A_{\text{c}}}{k_{12}}\right)^{\frac{2}{3}}\left[\dot{x}(t)\right]^{\frac{2}{3}} \tag{36}$$

Hence, the damping force during the compression stroke of the damper is

$$F_{\text{d}} = PA_{\text{c}} = A_{\text{c}}\left(\frac{A_{\text{c}}}{k_{12}}\right)^{\frac{2}{3}}\left[\dot{x}(t)\right]^{\frac{2}{3}} \tag{37}$$

We continue to define a constant

$$k_{13} = A_{\text{c}}\left(\frac{A_{\text{c}}}{k_{12}}\right)^{\frac{2}{3}} \tag{38}$$

to obtain

$$F_{\text{d}} = k_{13}\left[\dot{x}(t)\right]^{\frac{2}{3}} \tag{39}$$

Thus, the damping coefficient of the pantograph damper during compression can be written as

$$C_{\text{com}} = k_{13}\left[\dot{x}(t)\right]^{-\frac{1}{3}} \tag{40}$$

2.3.3 Simplified-parametric pantograph damper model

In engineering, it is feasible to assume that the pantograph is lowered with a constant speed before the orifices in the rod begin to be sequentially shielded by the guide seat. Thus, referring to Eq. (32), C_{ext} can be considered a constant in this process and defined as C_0.

However, when the orifices in the rod begin to be sequentially shielded, the damping coefficient

becomes large and complex; Eqs. (31) and (32) are available to describe the notably nonlinear behaviour in this process.

Similarly, we can assume that the pantograph is raised with a constant speed, and the speed is mainly determined by the performance of the pneumatic actuator. In addition, Eq. (39) indicates that the speed $\dot{x}(t)$ weakly affects the damping force, so F_d can be considered a constant. In fact, the compression shim-stack valve in the foot valve assembly is similar to a relief valve; when the damper is compressed, the damping forces are approximately constant and defined as F_{const}.

Therefore, a simplified-parametric pantograph damper model is proposed as follows

$$F_d = \begin{cases} C_0 \dot{x}(t), & \text{if } \dot{x}(t) \geq 0, \ -\dfrac{s_a}{2} \leq x(t) < \left(\dfrac{s_a}{2} - s_1\right), \\[2ex] k_{11}\left(1 + \dfrac{A_f^2}{A_n^2}\right)[\dot{x}(t)]^2, \ n = 0,1,\ldots,n-1, & \text{if } \dot{x}(t) \geq 0, \ \left(\dfrac{s_a}{2} - s_1\right) \leq x(t) \leq \dfrac{s_a}{2}, \\[2ex] F_{const}, & \text{if } \dot{x}(t) < 0. \end{cases} \tag{41}$$

Equation (41) is a concise model with apparent physical meaning to describe the nonlinear displacement-dependent damping characteristics of the pantograph damper. For a given type of pantograph damper, the second item in Eq. (41) can be subdivided according to the concrete configuration of the orifice network. For example, for the damper structure in Fig. 4, Eq. (41) can be concretely written as

$$F_d = \begin{cases} C_0 \dot{x}(t), & \text{if } \dot{x}(t) \geq 0, \ -\dfrac{s_a}{2} \leq x(t) < \left(\dfrac{s_a}{2} - s_1\right), \\[2ex] k_{11}\left(1 + \dfrac{A_f^2}{A_5^2}\right)[\dot{x}(t)]^2, & \text{if } \dot{x}(t) \geq 0, \ \left(\dfrac{s_a}{2} - s_1\right) \leq x(t) < \left[\left(\dfrac{s_a}{2} - s_1\right) + \Delta s_1\right], \\[2ex] k_{11}\left(1 + \dfrac{A_f^2}{A_4^2}\right)[\dot{x}(t)]^2, & \text{if } \dot{x}(t) \geq 0, \ \left[\left(\dfrac{s_a}{2} - s_1\right) + \Delta s_1\right] \leq x(t) < \left[\left(\dfrac{s_a}{2} - s_1\right) + \Delta s_2\right], \\[2ex] k_{11}\left(1 + \dfrac{A_f^2}{A_3^2}\right)[\dot{x}(t)]^2, & \text{if } \dot{x}(t) \geq 0, \ \left[\left(\dfrac{s_a}{2} - s_1\right) + \Delta s_2\right] \leq x(t) < \left[\left(\dfrac{s_a}{2} - s_1\right) + \Delta s_1 + \Delta s_2\right], \\[2ex] k_{11}\left(1 + \dfrac{A_f^2}{A_2^2}\right)[\dot{x}(t)]^2, & \text{if } \dot{x}(t) \geq 0, \ \left[\left(\dfrac{s_a}{2} - s_1\right) + \Delta s_1 + \Delta s_2\right] \leq x(t) < \left[\left(\dfrac{s_a}{2} - s_1\right) + 2\Delta s_2\right], \\[2ex] k_{11}\left(1 + \dfrac{A_f^2}{A_1^2}\right)[\dot{x}(t)]^2, & \text{if } \dot{x}(t) \geq 0, \ \left[\left(\dfrac{s_a}{2} - s_1\right) + 2\Delta s_2\right] \leq x(t) < \left[\left(\dfrac{s_a}{2} - s_1\right) + \Delta s_1 + 2\Delta s_2\right], \\[2ex] k_{11}\left(1 + \dfrac{A_f^2}{A_0^2}\right)[\dot{x}(t)]^2, & \text{if } \dot{x}(t) \geq 0, \ \left[\left(\dfrac{s_a}{2} - s_1\right) + \Delta s_1 + 2\Delta s_2\right] \leq x(t) \leq \dfrac{s_a}{2}, \\[2ex] F_{const}, & \text{if } \dot{x}(t) < 0. \end{cases} \tag{42}$$

where A_0–A_5 can be calculated using Eq. (27). In addition, according to Fig. 4, we have

$$s = s_0 + x(t), \ \dot{s} = \dot{x}(t) \tag{43}$$

Thus, the above simplified-parametric damper model can be easily coupled with the pantograph dynamics model and used for pantograph dynamics simulations.

2.3.4 Damper model validation

Both computer simulation and experimental research (Fig. 5) were performed to verify the proposed simplified-parametric pantograph damper model, and the results are shown in Fig. 6.

Fig. 6 compares the tested nominal-speed force vs. displacement (F_d-$x(t)$) characteristics with the simulated F_d-$x(t)$ characteristics of a high-speed rail pantograph hydraulic damper (Type: J6H36-02-00). Fig. 6 demonstrates that the test result is consistent with the simulation result, except for small biases in lower-level damping forces, and the biases are notably small and tolerable. In addition, the tested damping force sometimes appears less stable than the simulated damping force, which is common in practical product tests.

In section "a-b", the pantograph begins to be lowered, so the damper begins to extend. Because all

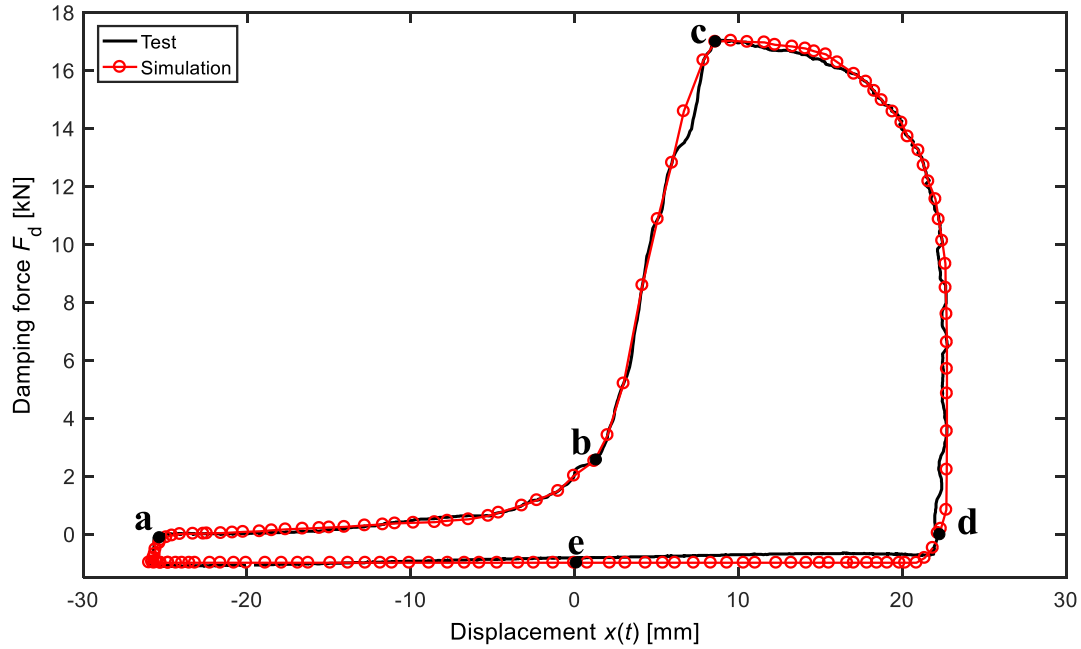**Fig. 5** Bench testing of a high-speed rail pantograph hydraulic damper

Fig. 6 Nominal-speed force vs. displacement (F_d-$x(t)$) characteristics of a high-speed rail pantograph hydraulic damper (Type: J6H36-02-00) with a harmonic excitation of displacement amplitude of ± 24.38 mm, a frequency of 0.65 Hz and a velocity amplitude of ± 0.1 m/s

orifices in the rod are available to charge the fluids, the damping force slowly increases although the excitation speed improves, so this is good for fast descending of the pantograph.

However, in section "b-c", the orifices in the rod begin to be sequentially shielded, so the damping forces drastically increase, and the descending speed of the pantograph quickly decreases. In section "c-d", although only the constant orifice in the inner tube works, the pantograph speed is approaching zero, so the damping force quickly descends to zero, and the pantograph is stopped and rests on the compartment roof.

In section "d-e-a", the pantograph is raised, so the damper is compressed. Because the compression shim-stack valve in the foot valve assembly plays a dominate role and acts as a relief valve in this process, the damper supplies a low-level and approximately constant damping force to the pantograph.

Thus, the proposed simplified-parametric model is validated by experimental results; the concise model accurately captures the nonlinear displacement-dependent damping characteristics of the pantograph hydraulic damper, and it appears more complete and accurate.

3. Effect of the damper characteristics on the pantograph dynamics

A detailed MATALB/Simulink model was developed using the deduced full mathematical model of the pantograph-catenary system in Section 2, with which the proposed simplified-parametric pantograph damper model was coupled. The parameter values in the MATALB/Simulink model for the dynamics simulation are summarized in the Appendix.

In the simulation, three cases of damper characteristics were used. Case 1 has high-level damping characteristics with C_0=15.57 kN s/m, maximum damping performance at section "b-c-d", which can be calculated by the second item in Eq. (41), and F_{const}=927.7 N. Case 2 has medium-level damping characteristics with C_0=9.50 kN s/m, medium damping performance at section "b-c-d", and F_{const}=480 N. Case 3 has low-level damping characteristics with C_0=4.00 kN s/m, minimum damping performance at section "b-c-d", and F_{const}=31 N.

3.1. Raising performance

When the pantograph is raised (the vehicle is stationary), the damper is compressed and works in section "d-e-a" as shown in Fig. 6, the F_{const} in Eq. (41) represents the level of damping in section "d-e-a".

Fig. 7 demonstrates the instantaneous current collector height and contact force of the pantograph when it is raised. Fig. 7(a) shows that the pantograph with a small F_{const} (Case 3) is quickly raised, but the collector fluctuates with large amplitudes, and for a long time after its first impact with the catenary, the contact (impact) forces during fluctuation are large, as shown in Fig. 7(b). The pantograph with a high-level F_{const} (Case 1) is quickly stabilized (Fig. 7(a)), although it is raised for a relatively longer time, and the contact forces are small and quickly stabilized (Fig. 7(b)). The performance of the pantograph with a medium-level F_{const} (Case 2) is between that of Cases 3 and 1.

Fig. 8 summarizes the concrete indices of the pantograph when it is raised and shows that Case 3 has the highest maximum contact force and longest raising time of the pantograph, Case 1 has the lowest maximum contact force and shortest raising time of the pantograph, and the indices in Case 2 are between those of Cases 3 and 1.
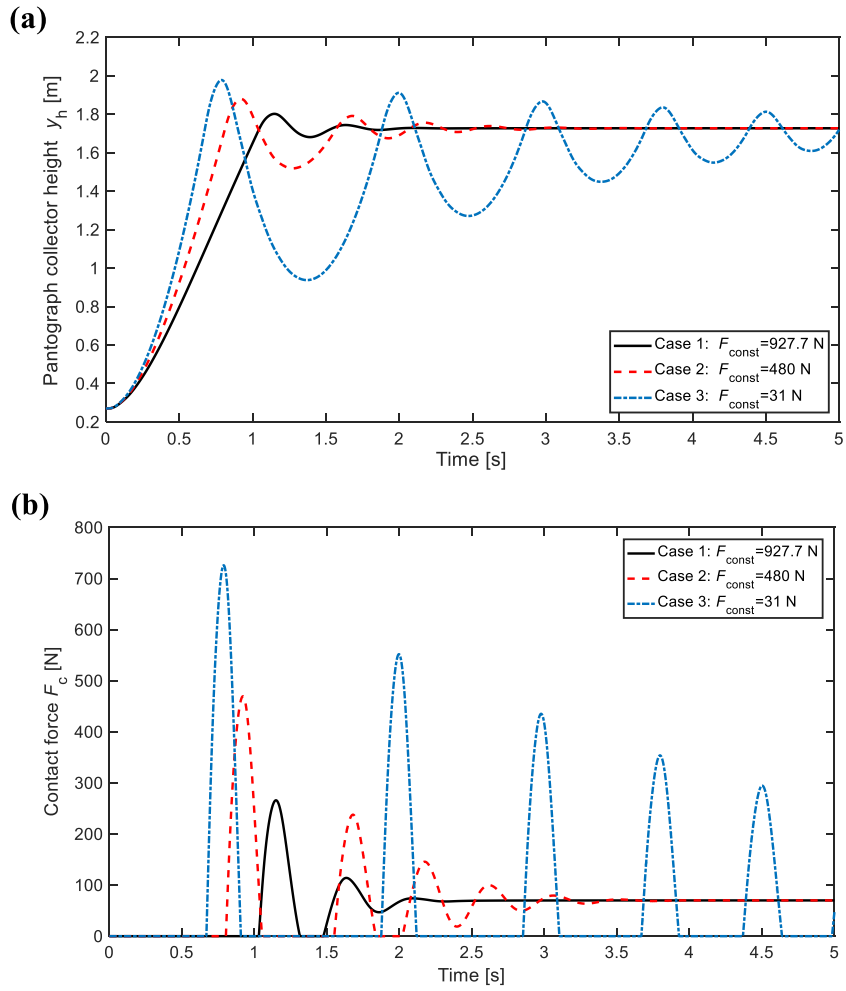
(a)

(b)

Fig. 7 Instantaneous collector height y_h (a) and contact force F_c (b) during the raising process of the pantograph
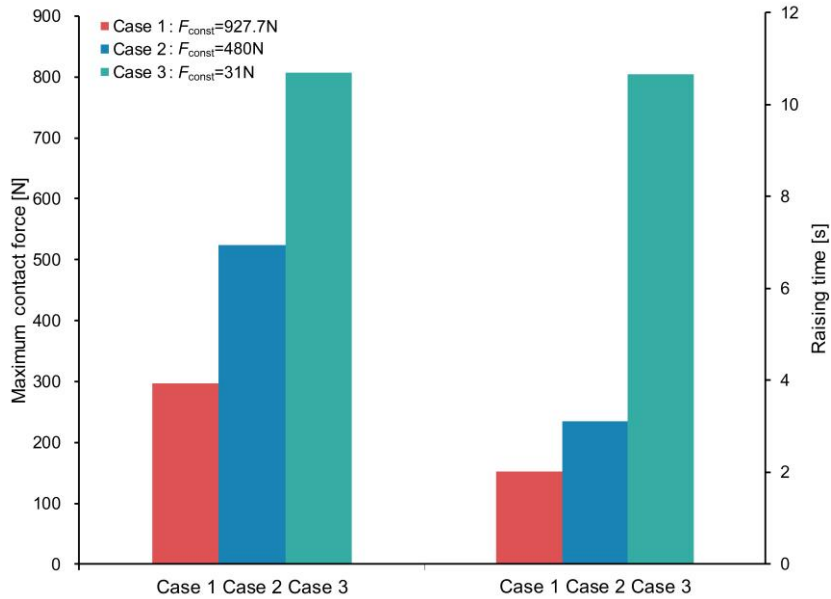

Fig. 8 Maximum contact force and raising time during the raising process of the pantograph

Thus, from the viewpoint of raising performance, F_{const} in the pantograph damper model Eq. (41) should not be designed to be too small or zero; otherwise, severe impacts between the pan-head and the catenary and a longer stabilization time of the pantograph will be induced; in other words, F_{const} has an optimal value.

3.2. Holding performance

When the pantograph is operating, i.e., the moving pantograph is holding with the catenary, the pantograph and hydraulic damper experience both high-frequency-low-amplitude vibrations and low-frequency-big-amplitude discrete disturbances. The hydraulic damper works in sections "a-b" and "d-e-a" (Fig. 6) during the holding process, so both parameters C_0 and F_{const} in Eq. (41) are crucial to the contact quality of the pan-head and catenary.

3.2.1 Pulse responses of the pantograph

The pulse responses of pantograph reflect the stabilization ability of the pantograph against disturbances. When the pantograph is subject to a positive force pulse input, the response of contact force F_c and its Power Spectrum Density (PSD) are demonstrated in Fig. 9. Fig. 9(a) shows that the pantograph with large C_0 and F_{const} (Case 1) is more easily stabilized in contact force than that with smaller C_0 and F_{const} (Cases 2 and 3). Fig. 9(b) also shows that the pantograph with large C_0 and F_{const} has weaker energies at the main frequencies of 2.6 Hz and 5.2 Hz than the pantograph with smaller C_0 and F_{const}.

Fig. 10 demonstrates the displacement pulse response of pantograph collector height y_h and its PSD when the pantograph is holding with the catenary, and indicates that the pantograph with large C_0 and F_{const} (Case 1) is more easily stabilized in collector height and has weaker energies at the main frequencies of 1 Hz and 2.6 Hz than that with smaller C_0 and F_{const} (Cases 2 and 3).
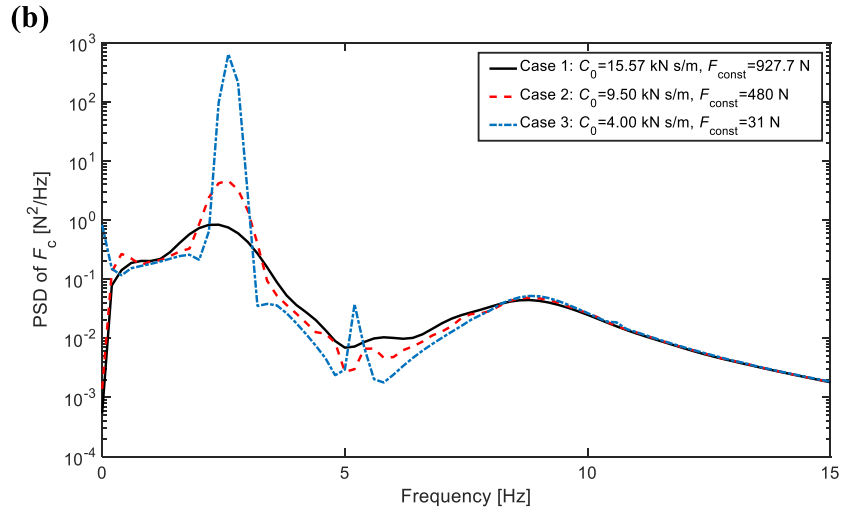
(a)

(b)
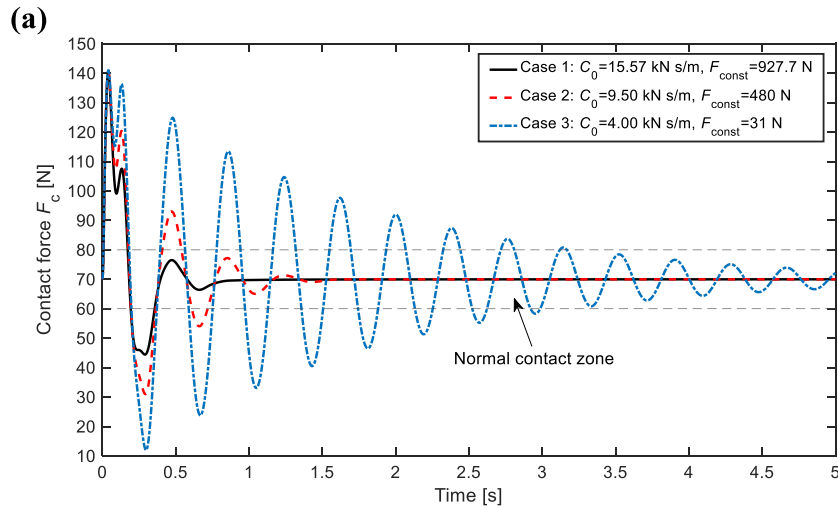
Fig. 9 Force pulse response of contact force F_c (a) and PSD of F_c (b) when the pantograph is holding with the catenary

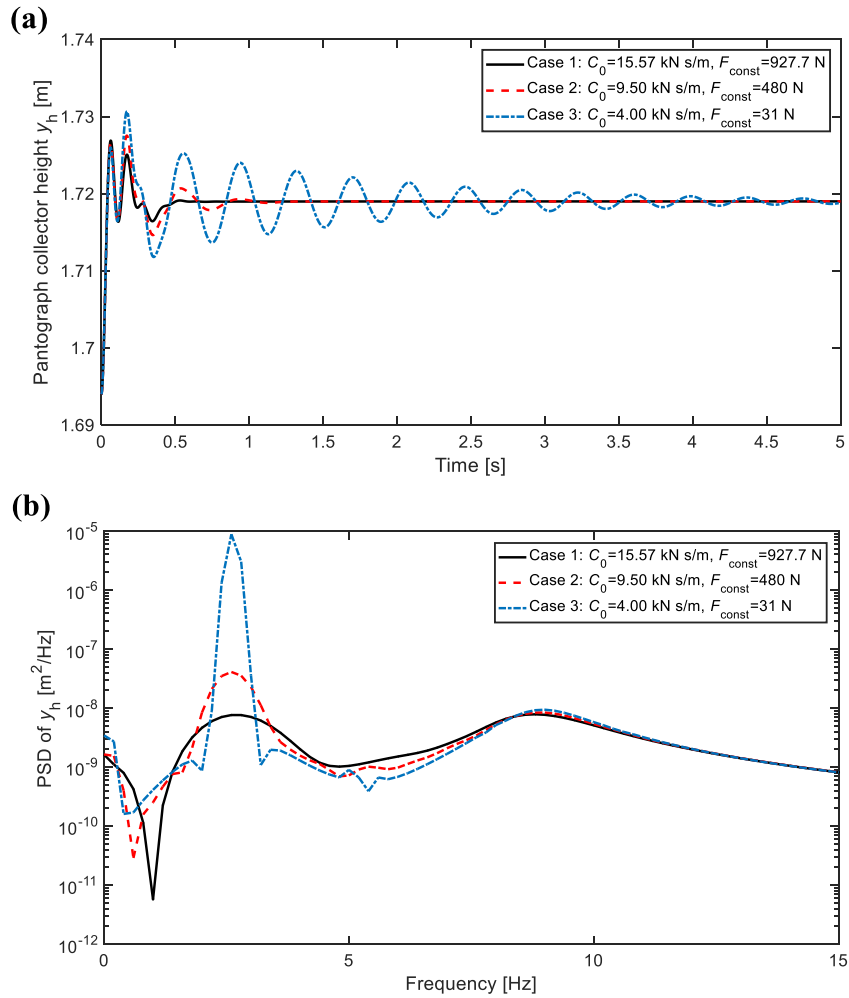**(a)**

(b)

Fig. 10 Displacement pulse response of collector height y_h (a) and PSD of y_h (b) when the pantograph is holding with the catenary

17

3.2.2 Dynamic contact performance of the pantograph and catenary

Fig. 11 demonstrates the instantaneous current collector height y_h and its PSD when the pantograph moves between the fifth and the seventh spans of the catenary at a speed of 200 km/h. The pantograph with large C_0 and F_{const} (Case 1) has lower vibration amplitudes in collector height (Fig. 11(a)) and weaker energy at the main frequency of 2.6 Hz (Fig. 11(b)) than that with smaller C_0 and F_{const} (Cases 2 and 3). However, the energy intensities at the main frequencies of 0.85 Hz and 1.77 Hz do not show remarkable differences among the three cases.
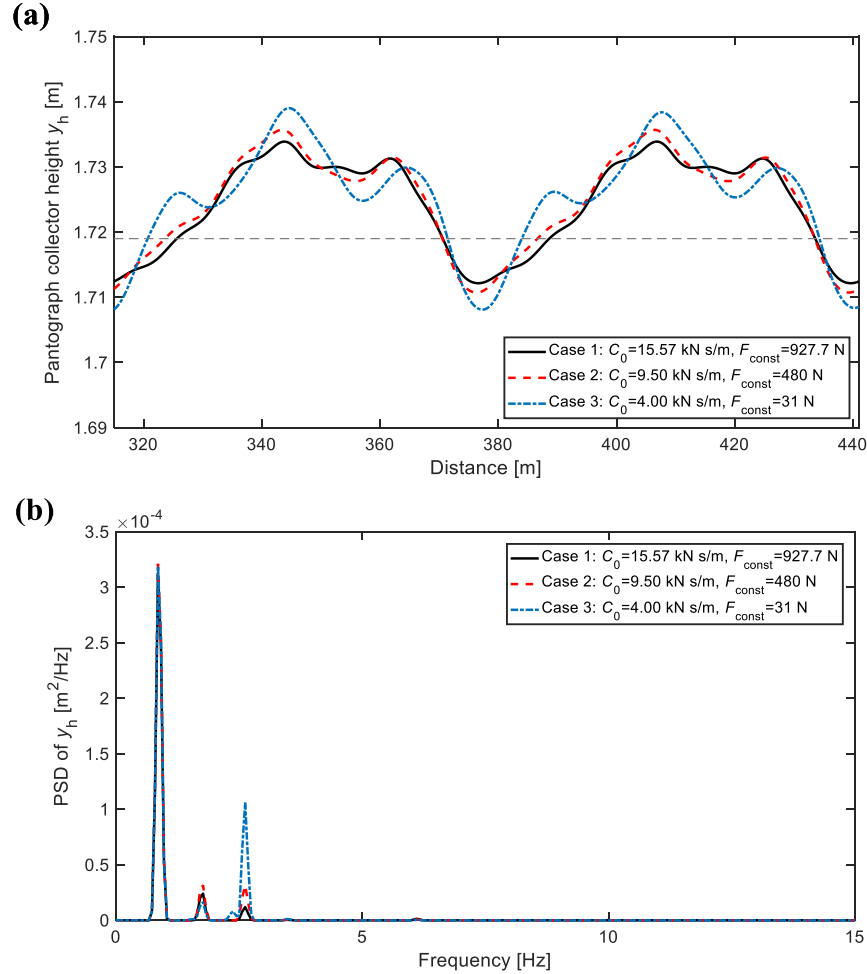
(a)

(b)

Fig. 11 Instantaneous current collector height y_h (a) and PSD of y_h (b) when pantograph moves between the fifth to the seventh spans of the catenary at a speed of 200 km/h

Fig. 12 demonstrates the instantaneous contact force F_c and its PSD when the pantograph moves between the fifth and the seventh spans of the catenary at a speed of 200 km/h. Fig. 12 shows that the pantograph with large C_0 and F_{const} (Case 1) has lower-level fluctuating amplitudes in contact force (Fig. 12(a)) and weaker energy at the main frequency of 2.6 Hz (Fig. 12(b)) than that with smaller C_0 and F_{const} (Cases 2 and 3). The differences in energy intensity at other main frequencies are not obvious among the three cases.
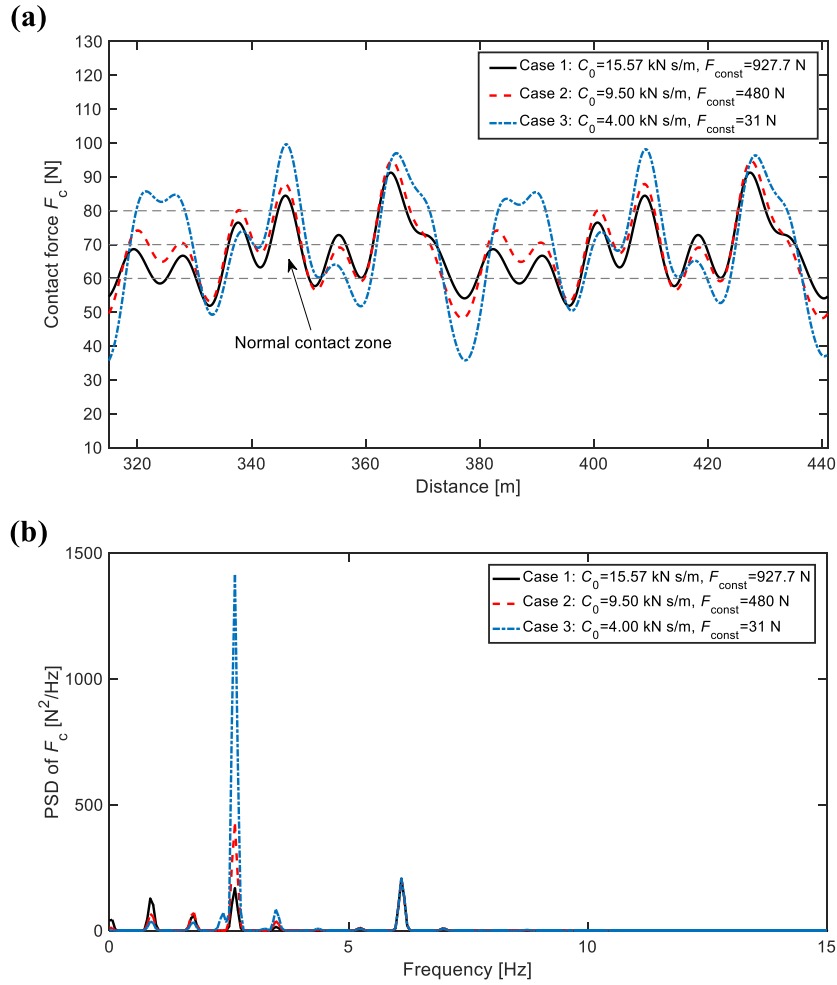
18

Fig. 12 Instantaneous contact force F_c (a) and PSD of F_c (b) when the pantograph moves between the fifth to the seventh spans of the catenary at a speed of 200 km/h
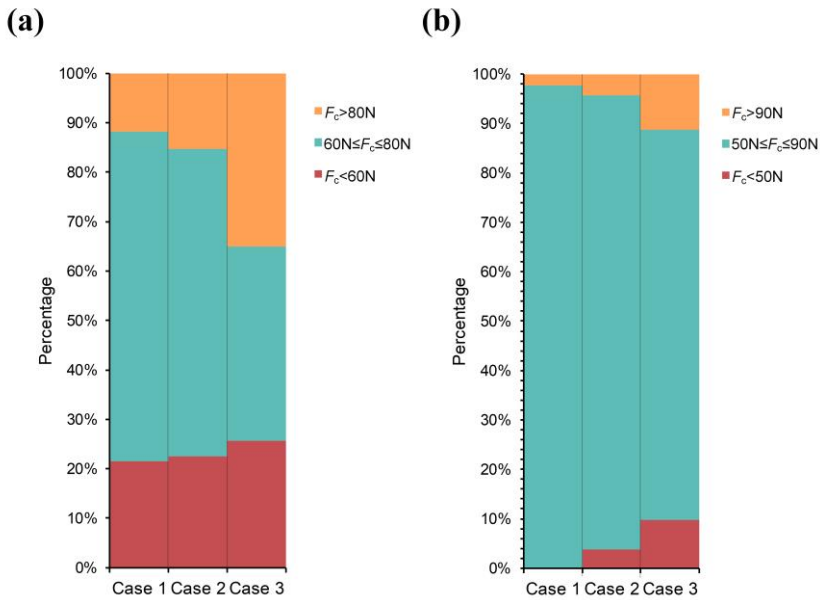

Fig. 13 Normal **c**ontact force distributions (a) and extreme **c**ontact force distributions (b) of the pantograph

Fig. 13 summarizes and compares the contact force distributions of the pantograph when the pantograph has different levels of C_0 and F_{const}. When 60 N $\leq F_c \leq$ 80 N, the contact force is considered in the normal [27] contact zone, as shown in Figs. 9(a) and 12(a). When $F_c > 80$ N or $F_c < 60$ N, the contact force is considered higher or lower than the normal value. If $F_c > 90$ N, the contact force is considered too high and may damage the pan-head and catenary; if $F_c < 50$ N, the contact force is considered too low and the pan-head is about to lose contact with the catenary.

Fig. 13 shows that the percentage of normal contact forces of the pantograph with large C_0 and F_{const} (Case 1) is over 66.5% (Fig. 13(a)) and that of extreme contact forces is below 2.5% (Fig. 13(b)). However, the percentage of normal contact forces of the pantograph with small C_0 and F_{const} (Case 3) is only 39.3% (Fig. 13(a)) and that of extreme contact forces exceeds 21% (Fig. 13(b)). The percentages of Case 2 are between those of Cases 3 and 1.

Thus, from the viewpoint of contact quality, large C_0 and F_{const} in the pantograph damper model (Eq. (41)) can increase the percentage of normal contact forces and reduce that of extreme contact forces. In other words, it can improve the pantograph-catenary contact quality. In engineering, C_0 and F_{const} should not be designed to be too small or zero.

3.3. Lowering performance

When the pantograph is lowered (the vehicle can be stationary or moving), the damper is stretched and works in section "a-b-c-d" as shown in Fig. 6. If we divide section "a-b-c-d" into "a-b" and "b-c-d", C_0 represents the damping performance in section "a-b", and the second item in Eq. (41) represents the damping performance in section "b-c-d".

Figs. 14(a) and (b) show the instantaneous height y_e of joint E and velocity $\dot{y}_e$ of joint E when the pantograph is lowered. As an example (Case 1), Fig. 14(b) shows the lowering process of the pantograph; sections "a-b" and "b-c-d" correspond to sections "a-b" and "b-c-d" in Fig. 6, respectively. In section "a-b", the pantograph descends against a relatively small damping of C_0, so the pantograph speed increases; however, in section "b-c-d", because the pantograph is subject to a very large nonlinear damping, the pantograph speed is drastically reduced in section "b-c" and decreases to zero in section "c-d" when the pantograph impacts the base frame. Fig. 14(b) also illustrates the lowering times t_1 in section "a-b" and t_2 in section "b-c-d"; the sum of t_1 and t_2 is equal to the total lowering time of the pantograph.

Fig. 14(b) indicates that speed of the pantograph with high-level damping (Case 1) is quickly reduced but requires a longer time to reach zero, whereas the speed of the pantograph with low-level damping (Case 3) is slowly reduced but quickly reaches zero. However, because of the considerable impact of the pantograph and base frame in Case 3, the final speeds drastically fluctuate. The final impact intensity is also observed in Fig. 14(c), where the pantograph with low-level damping (Case 3) has the largest velocity
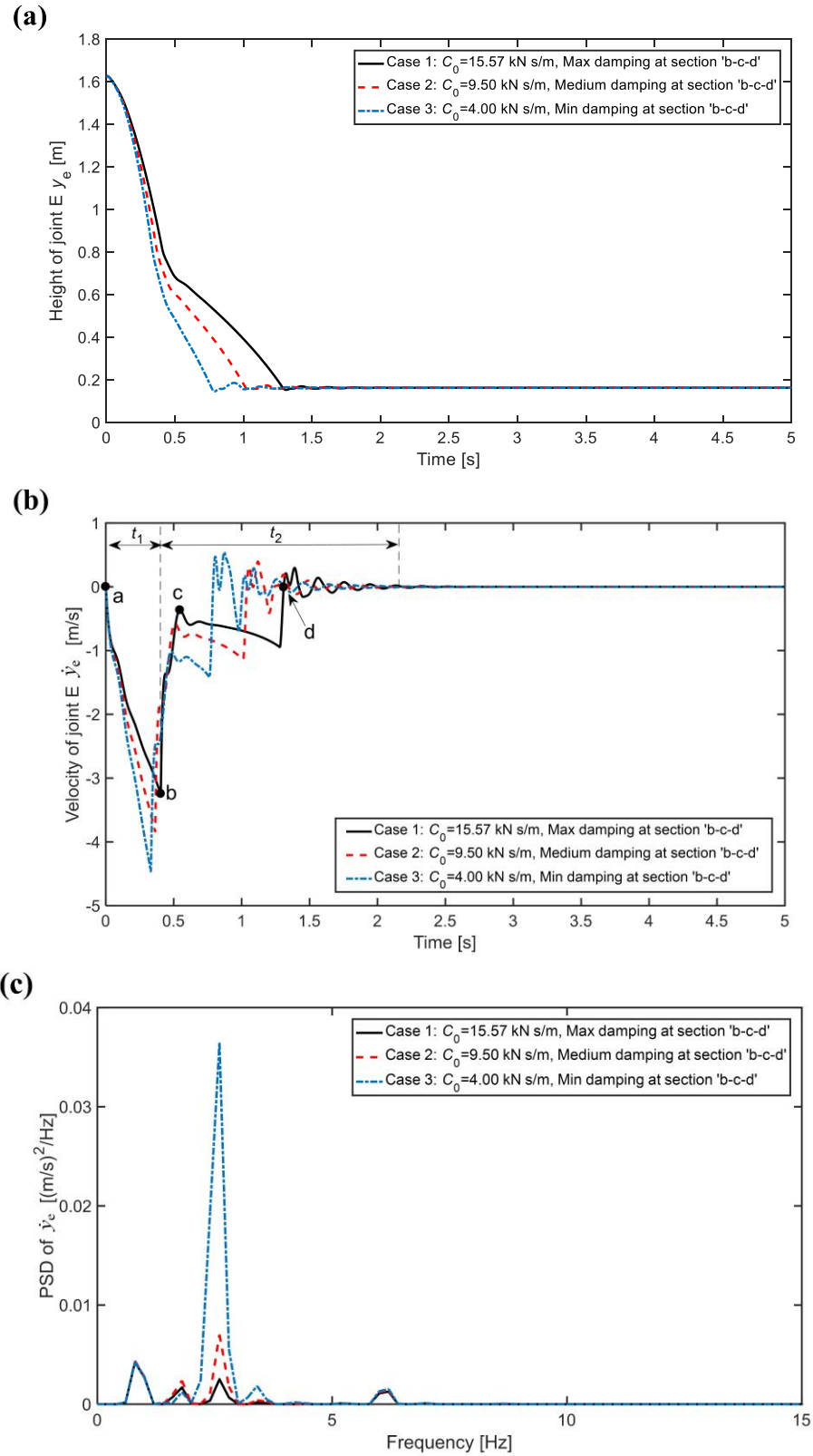
(a)

(b)

(c)

Fig. 14 Instantaneous height y_e (a) and velocity $\dot{y}_e$ (b) of joint E and PSD of $\dot{y}_e$ (c) when the pantograph is lowered

impact energy at the main frequency of 2.6 Hz.

21

Fig. 15 demonstrates the instantaneous acceleration $\ddot{y}_e$ of joint E and PSD of $\ddot{y}_e$ when the pantograph is lowered. Fig. 15(a) shows that the pantograph with a high-level damping (Case 1) has the largest maximum acceleration in the speed reduction process, i.e., section "b-c" of Fig. 14(b), and the smallest maximum impact acceleration in the final process, i.e., section "c-d" of Fig. 14(b). Fig. 15(a) also shows that the pantograph with low-level damping (Case 3) has the largest maximum impact acceleration in the final process. In the frequency domain, Fig. 15(b) obviously shows that the pantograph in Case 3 has the largest acceleration impact energies at the main frequencies of 9.2 Hz and 13.8 Hz.

(a)

(b)
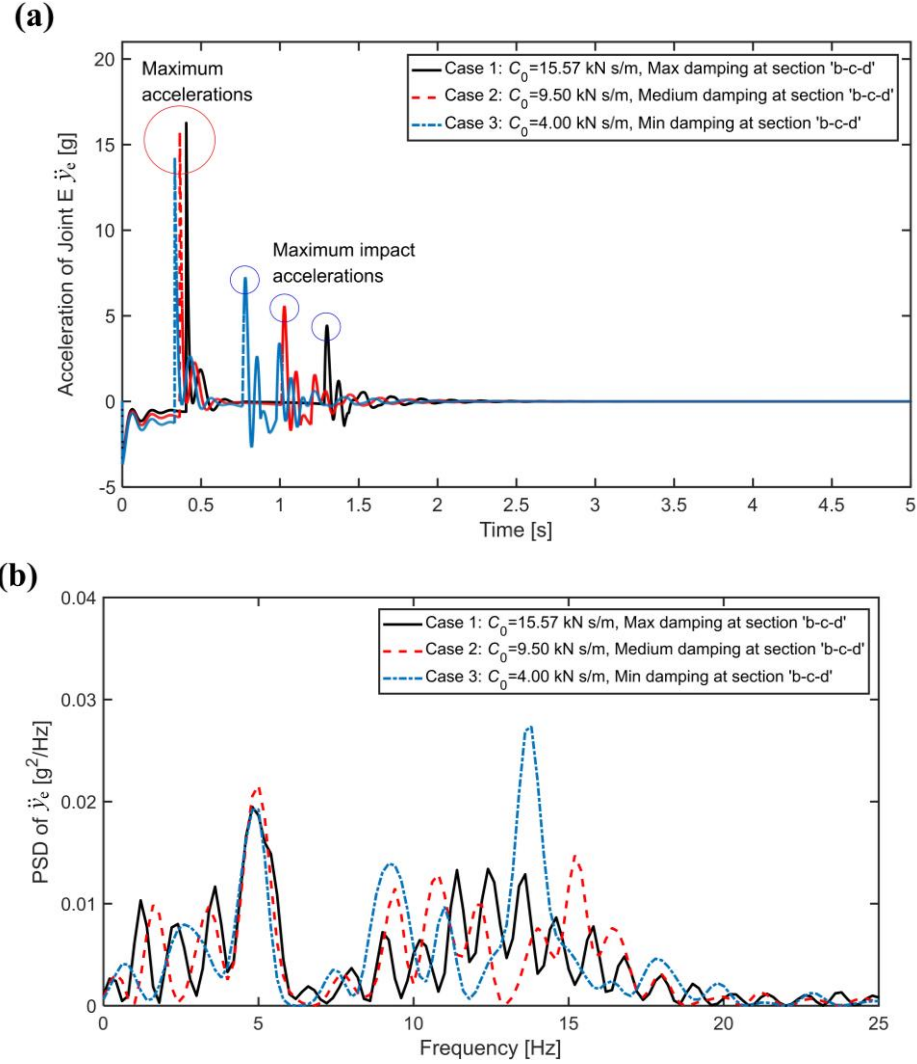
Fig. 15 Instantaneous acceleration $\ddot{y}_e$ of joint E (a) and PSD of $\ddot{y}_e$ (b) when the pantograph is lowered

Fig. 16 demonstrates the instantaneous vertical momentum and PSD of the vertical momentum of the pantograph when the pantograph is lowered. In the main section of speed reduction "b-c", the pantograph with a high-level damping (Case 1) has the largest vertical momentum (Fig. 16(a)) and vertical momentum energies (Fig. 16(b)) at the main frequencies of 0.2 Hz and 1.2 Hz. However, in the final impact process, the pantograph with low-level damping (Case 3) has the largest vertical momentum (Fig. 16(a)) and vertical

momentum energies (Fig. 16(b)) at the main frequency of 4.2 Hz.

Fig. 17 summarizes the lowering time in terms of t_1 and t_2, maximum acceleration and maximum impact acceleration of the pantograph during the lowering process. Fig. 17(a) indicates that the differences in lowering time t_1 in the first stage "a-b" are not obvious among the three cases, so the damping coefficient C_0 has no obvious effect on the lowering time of the pantograph. Fig. 17(a) also indicates that the higher level of damping in section "b-c-d" of the damper corresponds to a longer total lowering time of the pantograph. In other words, the damping performance in section "b-c-d" (Fig. 6 and the second item in Eq. (41)) of the damper has an obvious effect on the lowering time of the pantograph.
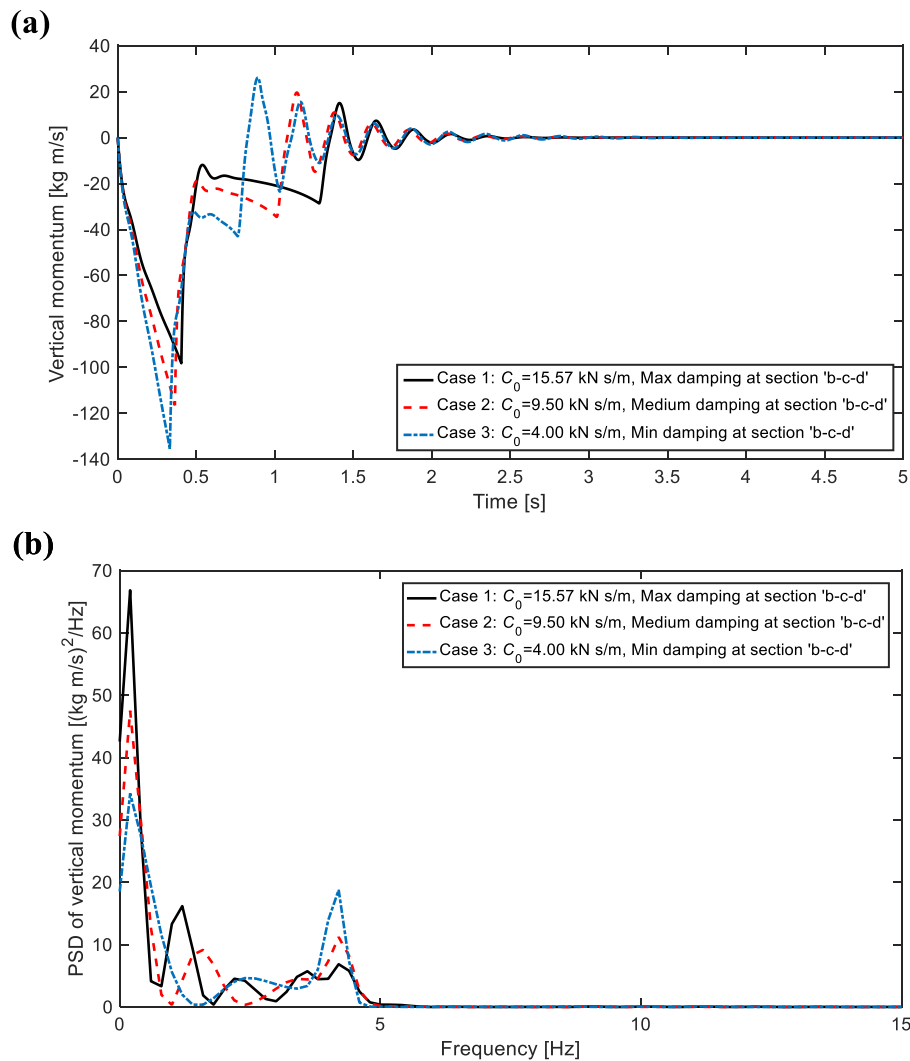

Fig. 16 Instantaneous vertical momentum (a) and PSD of the vertical momentum (b) of the pantograph when the pantograph is lowered
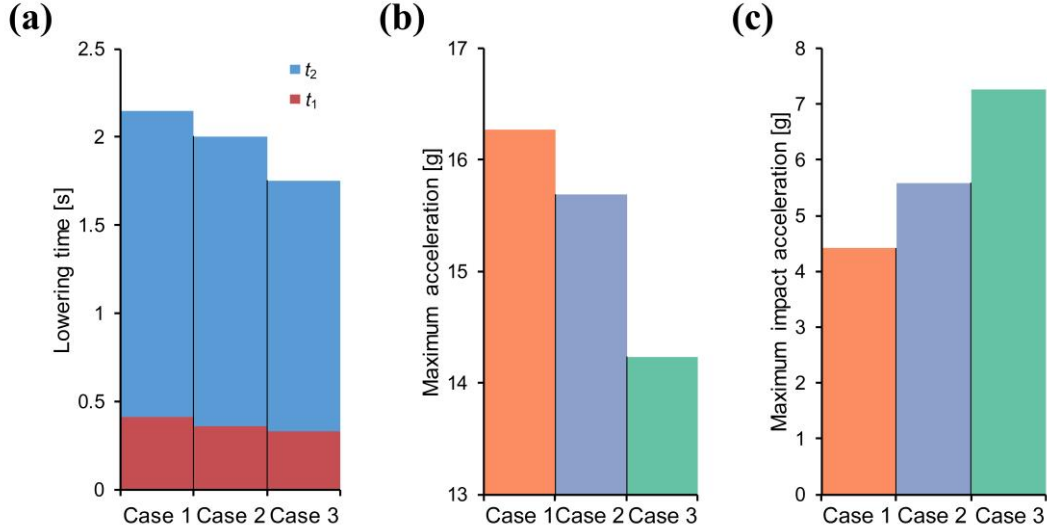
Fig. 17 Lowering time in terms of t_1 and t_2 (a), maximum acceleration (b) and maximum impact acceleration (c) of the pantograph

Figs. 17(b) and (c) show that the higher level of damping in section "b-c-d" of the damper corresponds to the larger maximum acceleration and smaller maximum impact acceleration of the pantograph. In other words, the speed of the pantograph with high-level damping (Case 1) is quickly reduced, and the pantograph is more softly dropped on the base frame, but a longer total lowering time (Fig. 17(a)) is induced by the high-level damping.

Therefore, from the viewpoint of lowering performance, the damping coefficient C_0 in section "a-b" of the damper has no obvious effect on the lowering time of the pantograph, whereas the nonlinear damping characteristics in section "b-c-d" of the damper, which are described by the second item in Eq. (41), have dominating effects on the total lowering time, maximum acceleration and maximum impact acceleration of the pantograph. Thus, within the constraint of the total lowering time, increasing the damping characteristics in section "b-c-d" will obviously improve the lowering performance of the pantograph.

4. Concluding remarks

(1) A new simplified-parametric model was proposed to describe the nonlinear displacement-dependent damping characteristics of the railway pantograph hydraulic damper and validated by experimental results. A full mathematical model of the pantograph-catenary system, which incorporated the new pantograph damper model, was established to simulate the effect of the damping characteristics on the pantograph dynamics, which includes the raising, holding and lowering performance of the pantograph.

(2) Large F_{const} and C_0 in the pantograph damper model have three benefits: increased response quality of the pantograph when the pantograph is raised; avoidance of excessive impact between the pan-head and the catenary; and improved pantograph-catenary contact quality by increasing the percentage of normal contact forces and reducing the percentage of extreme contact forces. Let alone, a large C_0 has no obvious

effect on the lowering time of the pantograph; thus, in engineering design, C_0 and F_{const} should not be too small or zero.

(3) The nonlinear damping characteristics described by the second item in the new damper model have dominating effects on the total lowering time, maximum acceleration and maximum impact acceleration of the pantograph. Thus, within the constraint of total lowering time, increasing the second item damping characteristics of the damper will obviously improve the lowering performance of the pantograph and reduce excessive impact between the pantograph and its base frame.

(4) The proposed concise pantograph hydraulic damper model appears to be more complete and accurate than the previous single-parameter model, so it is more useful in pantograph-catenary dynamics simulations and further parameter optimizations. The obtained simulation results are also useful and instructive for optimal specification of pantograph hydraulic dampers. However, this work was performed by neglecting the performance and time delay of the pneumatic actuating system, so it will be interesting to incorporate the pneumatic system dynamics in the next study.

Acknowledgement

Appendix:

Parameters and values in the pantograph-catenary dynamics modelling and simulation

Notation (Unit)	Description	Value	Remarks
m_1 (kg)	Coupling rod mass	3.90	
J_1 (kg m^2)	Coupling rod moment of inertia	1.88	
l_1 (m)	Coupling rod length	1.20	
l_{m1} (m)	Length from the center of gravity of the coupling rod to joint A	6.03E-001	
θ_2 (°)	Angle from the coupling rod to level	Variable	
l_2 (m)	Length of connecting rod BC	3.40E-001	
θ_1 (°)	Angle from the connecting rod BC to level	Variable	

m_3 (kg)	Lower arm mass	2.10E+001
J_3 (kg m^2)	Lower arm moment of inertia	1.75E+001
l_3 (m)	Lower arm length	1.58
l_{m3} (m)	Length from the center of gravity of the lower arm to joint D	7.93E-001
α (°)	Rising angle of the lower arm (pantograph)	Variable
h_0 (m)	Vertical distance of joints A and D	1.30E-001
l_0 (m)	Horizontal distance of joints A and D	7.20E-001
m_4 (kg)	Upper arm mass	1.60E+001
J_4 (kg m^2)	Upper arm moment of inertia	2.02E+001
l_4 (m)	Upper arm length	1.95
l_{m4} (m)	Length from the center of gravity of the upper arm to joint C	9.14E-001
β (°)	Angle from the connecting rod BC to upper arm	1.15E+001
y_e (m)	Height of joint E	Variable
m_h (kg)	Pan-head mass	5.00
k_h (N/m)	Equivalent stiffness of the pan-head suspension	7.60E+003
c_h (N/m)	Equivalent damping coefficient of the pan-head suspension	5.00E+001
l_h (m)	Height between the collector and joint E	1.00E-001
y_h (m)	Height of the pantograph collector	Variable
y_c (m)	Height of the catenary	1.70
L_c (m)	Span length of the catenary	6.30E+001
L_d (m)	Dropper interval	9.00
k_c (N/m)	Catenary stiffness	Variable
k_0 (N/m)	Static stiffness of the catenary	3.6845E+003
a_1	Coefficient	4.665E-001
a_2	Coefficient	8.32E-002
a_3	Coefficient	2.603E-001
a_4	Coefficient	-2.801E-001

Symbol	Description	Value	Notes
a_1	Coefficient	-3.364E-001	
F_c (N)	Pantograph-catenary contact force	Variable	
v (km/h)	Vehicle speed	2.00E+002	
L	Lagrangian function	Function	
T (J)	Kinetic energy of the framework	Variable	
U (J)	Potential energy of the framework	Variable	
G_F (N m)	Generalized force	Variable	
J_f (kg m^2)	Equivalent moment of inertia of the framework	Variable	
U_f (N s^2/m)	Coefficient of $\dot{y}_e^2$ in dynamic model of the framework	Variable	
F_f (N m)	Equivalent generalized force of the framework	Variable	
M_α (N m)	Uplift moment	Variable	
F_u (N)	Static uplift force	7.00E+001	
C_f (N s/m)	Equivalent damping coefficient of the framework	Variable	
F_d (N)	Damping force of the hydraulic damper	Variable	
g (m/s^2)	Acceleration of gravity	9.80	
l (m)	Length of the connection rod DP	1.80E-001	
x_d (m)	Horizontal distance between point P and joint N	3.50E-001	
y_d (m)	Vertical distance between joints D and N	0.00	Joints D and N are on the same level
s (m)	Instantaneous length of the hydraulic damper	Variable	
γ (°)	Angle from the connection rod DP to lower arm	5.56E+001	
s_0 (m)	Hydraulic damper length when the pantograph is completely raised	3.65E-001	
$x(t)$ (m)	Instantaneous displacement of the hydraulic damper	Variable	
k_1-k_{13}	Coefficients	Variable	The unit depends on concrete meaning of the coefficient
t (s)	Time	Variable	
A_c (m^2)	Pressure action area of the piston during the extension stroke of the damper	Variable	

Symbol	Description	Value	Note
A_f (m^2)	Cross-section area of the orifices in the rod for fluid outflow	Variable	
A_1-A_n (m^2)	Changeable cross-section area of the orifices in the rod for fluid inflow	Variable	n=1, 2, … 6 in this work
A_x (m^2)	Pressure action area of the piston during the compression stroke of the damper	Variable	
C_{com} (N s/m)	Damping coefficient of the damper during compression	Variable	
C_{d1}	Discharge coefficient of the orifice	7.20E-001	
C_{d2}	Discharge coefficient of the shim-stack valve	6.10E-001	
C_e	Equivalent-pressure correction factor	3.15E-001	FEA identified
C_{ext} (N s/m)	Damping coefficient of the damper during extension	Variable	
C_w (m^6/N)	Deflection coefficient of the shim	Variable	
C_0 (N s/m)	Initial damping coefficient of the damper during extension	Variable	
D (m)	Piston diameter	3.60E-002	
E (Pa)	Elastic modulus of the shim	2.00E+011	
F_{const} (N)	Damping force of the damper during compression	Variable	
P (Pa)	Instantaneous working pressure of the damper	Variable	
P_i (Pa)	Instantaneous pressure in the hollow passage of the rod	Variable	
Q_{work} (m^3/s)	Instantaneous working flow of the damper	Variable	
d (m)	Rod diameter	1.58E-002	
d_0 (m)	Diameter of the orifice in the inner tube	6.00E-004	
d_1 (m)	Diameter of the orifice in the rod for fluid inflow	1.10E-003	
d_2 (m)	Diameter of the orifice in the rod for fluid outflow	1.20E-003	
d_3 (m)	Diameter of the orifice in the rod for fluid outflow	1.10E-003	
d_4 (m)	Diameter of the orifice in the rod for fluid outflow	1.10E-003	
h_1-h_n (m)	Thickness of the shims in a shim-stack	5.00E-004	
r_s (m)	Outer radius of the shim	8.00E-003	
s_a (m)	Displacement amplitude of the damper	5.00E-002	
s_1 (m)	Distance from the first orifice in the rod to point (0, s_a/2)	2.10E-002	
Δs_1 (m)	Orifice interval	1.40E-003	
Δs_2 (m)	Orifice interval	3.20E-003	
ρ (kg/m^3)	Oil density	8.75+002	

References

1. Zhang, W.H.: The development of China's high-speed railway systems and a study of the dynamics of coupled systems in high-speed trains. IMechE, Part F: J. Rail & Rapid Transit. **228**(4), 367–377 (2014)

2. Mellado, A.C., Gómez, E., Viñolas, J.: Advances on railway yaw damper characterisation exposed to small displacements. Int. J. Heavy Veh. Syst. **13**(4), 263–280 (2006)

3. Alonso, A., Giménez, J.G., Gomez, E.: Yaw damper modelling and its influence on railway dynamic stability. Veh. Syst. Dyn. **49**(9), 1367–1387 (2011)

4. Wang, W.L., Yu, D.S., Huang, Y., Zhou, Z., Xu, R.: A locomotive's dynamic response to in-service parameter variations of its hydraulic yaw damper. Nonlinear Dyn. **77**(4), 1485– 1502 (2014)

5. Wang, W.L., Zhou, Z.R., Yu, D.S., Qin, Q.H., Iwnicki, S.: Rail vehicle dynamic response to the nonlinear physical in-service model of its secondary suspension hydraulic dampers. Mechanical Systems and Signal Processing. **95**, 138–157 (2017)

6. Oh, J.S., Shin, Y.J., Koo, H.W., Kim, H.C., Park, J., Choi, S.B.: Vibration control of a semi-active railway vehicle suspension with magneto-rheological dampers. Advances in Mechanical Engineering. **8**(4), 1–13 (2016)

7. Stein, G.J., Múčka, P., Gunston, T.P.: A study of locomotive driver's seat vertical suspension system with adjustable damper. Veh. Syst. Dyn. **47**(3), 363–386 (2009)

8. Croft, B.E., Jones, C.J.C., Thompson, D.J.: Modelling the effect of rail dampers on wheel–rail interaction forces and rail roughness growth rates. J. Sound Vib. **323**, 17–32 (2009)

9. Pombo, J., Ambrósio, J.: Influence of pantograph suspension characteristics on the contact quality with the catenary for high speed trains. Computers and Structures. **110–111**, 32–42 (2012)

10. Lopez-Garcia, O., Carnicero, A., Maroño, J.L.: Influence of stiffness and contact modelling on catenary–pantograph system dynamics. J. Sound Vib. **299**(4), 806–821 (2007)

11. Kim, J.W., Chae, H.C., Park, B.S., Lee, S.Y., Han, C.S., Jang, J.H.: State sensitivity analysis of the pantograph system for a high-speed rail vehicle considering span length and static uplift force. J. Sound Vib. **303**(3–5), 405–427 (2007)

12. Cho, Y.H.: Numerical simulation of the dynamic responses of railway overhead contact lines to a moving pantograph considering a nonlinear dropper. J. Sound Vib. **315**, 433–454 (2008)

13. Cho, Y.H., Lee, K., Park, Y., Kang, B., Kim, K.: Influence of contact wire pre-sag on the dynamics of pantograph – railway catenary. Int. J. Mech. Sci. **52**(11), 1471–1490 (2010)

14. Bautista, A., Montesinos, J., Pintado, P.: Dynamic interaction between pantograph and rigid overhead lines using a coupled FEM – multibody procedure. Mechanism and Machine Theory. **97**, 100–111 (2016)

15. Gregori, S., Tur, M., Nadal, E., Aguado, J.V., Fuenmayor, F.J., Chinesta, F.: Fast simulation of the pantograph – catenary dynamic interaction. Finite Elements in Analysis and Design. **129**, 1–13 (2017)

16. Zhang, W.H., Liu, Y., Mei, G.M.: Evaluation of the coupled dynamical response of a pantograph-catenary system: contact force and stresses. Veh. Syst. Dyn. **44**(8), 645–658 (2006)

17. Benet, J., Cuartero, N., Cuartero, F., Rojo, T., Tendero, P., Arias, E.: An advanced 3D-model for the study and simulation of the pantograph catenary system. Transportation Research Part C. **36**, 138–156 (2013)

18. Song, Y., Ouyang, H.J., Liu, Z.G., Mei, G.M., Wang, H.R., Lu, X.B.: Active control of contact force for high-speed railway pantograph-catenary based on multi-body pantograph model. Mechanism and Machine Theory. **115**, 35–59 (2017)

19. Zhou, N., Zhang, W.H.: Investigation on dynamic performance and parameter optimization design of pantograph and catenary

system. Finite Elements in Analysis and Design. **47**(3), 288–295 (2011)

20. Ma, G.N.: A study on the pantograph-catenary system. Master's degree thesis, South-west Jiaotong University (2009) (in Chinese)

21. Lee, J.H., Kim, Y.G., Paik, J.S., Park, T.W.: Performance evaluation and design optimization using differential evolutionary algorithm of the pantograph for the high-speed train. J. Mech. Sci. Tech. **26**(10), 3253–3260 (2012)

22. Ambrósio, J., Pombo, J., Pereira, M.: Optimization of high-speed railway pantographs for improving pantograph-catenary contact. Theoretical and Applied Mechanics Letters. **3**(1), 013006 (2013)

23. Kim, J.W., Yu, S.N.: Design variable optimization for pantograph system of high-speed train using robust design technique. Int. J. Precis. Eng. Man. **14**(2), 267–273 (2013)

24. Zhang, W.H.: Dynamic Simulation of Railway Vehicles. China Railway Publishing House, Beijing (2006) (in Chinese)

25. Guo, J.B.: Stable current collection and control for high-speed locomotive pantograph. Ph.D. thesis, Beijing Jiaotong University (2006) (in Chinese)

26. Wang, W.L., Zhou, Z.R., Cao, X.C., Iwnicki, S.: Physical modelling the displacement-dependent nonlinear characteristics of a high-speed rail pantograph hydraulic damper. Int. J. Eng. Sci. (Submitted)

27. Chinese National Standard: Railway applications – Rolling stock – Pantographs – Characteristics and tests – Part 1: Pantographs for mainline vehicles, GB/T 21561.1–2008 (2008) (in Chinese)